

We are IntechOpen, the world's leading publisher of Open Access books Built by scientists, for scientists

4,800

Open access books available

122,000

International authors and editors

135M

Downloads

Our authors are among the

154

Countries delivered to

TOP 1%

most cited scientists

12.2%

Contributors from top 500 universities



WEB OF SCIENCE™

Selection of our books indexed in the Book Citation Index
in Web of Science™ Core Collection (BKCI)

Interested in publishing with us?
Contact book.department@intechopen.com

Numbers displayed above are based on latest data collected.
For more information visit www.intechopen.com



Nondestructive Characterization of Residual Stress Using Micromagnetic and Ultrasonic Techniques

Madalina Rabung, Meisam Amiri, Michael Becker, Melanie Kopp, Ralf Tschuncky, Ines Veile, Fabian Weber, Miriam Weikert-Müller and Klaus Szielasko

Abstract

Material processing and service loads in different lifecycle stages of a product—ranging from semi-finished goods to operating structures—lead to an unfavorable superposition of residual stresses, especially of micro- and macro-residual stresses. Whereas near-surface compressive stress is often desired as it prolongs the useful service life, undesired, steep stress gradients and tensile stress at the surface promote the occurrence of cracks and wear during operation, ultimately leading to expensive and possibly dangerous premature component failure. Reliable management of the residual stress condition significantly contributes to the assessment and optimization of a part's or component's lifetime. Therefore, the nondestructive evaluation of residual stress in objects of different scales reaching from laboratory samples over semi-finished products up to operating components and structures has gained significant importance in the latest decades. Micromagnetic and ultrasonic methods are based on the interaction of an external magnetic field or an ultrasonic wave, respectively, with the material's microstructure and residual stress fields on different scales and in different depths from the material surface. The present contribution provides an overview regarding the local and volumetric measurement, characterization and evaluation of macro- and micro-residual stress by means of micromagnetic and ultrasonic techniques.

Keywords: residual stress, nondestructive, micromagnetic, ultrasound, EMAT

1. Introduction

Residual stress is the totality of internal forces per area acting upon a boundary surface of a volume within a material, thereby maintaining the current size and shape of a given object under the absence of external loads [1, 2]. Depending on the range of constant stress value and direction, residual stress in polycrystals is divided into first kind (constant across larger distance, e.g., across several crystals/grains), second kind (constant across smaller distance, e.g., within a crystal/grain) and third kind (varies on the submicroscopic scale, e.g., from atom to atom) [2].

Although best expressed as a tensor, industrial practice often demands for simplified residual stress values regarding one or a few relevant directions, such as those most critical under the expected service load.

Residual stress has significant impact on product quality and useful service life, as it affects the product geometry and processability (strip steel being just one example), the tendency to crack appearance (e.g., after hardening or forming) as well as the fatigue lifetime. The present contribution discusses micromagnetic and ultrasonic techniques that are industrially applied for nondestructive stress measurement.

2. Theoretical background on the used nondestructive methods

2.1 Micromagnetic techniques

2.1.1 Magnetic structure

The prerequisite for the application of micromagnetic nondestructive testing methods is a ferromagnetic behavior of the material to be tested. Such ferromagnetic materials have a characteristic domain structure. Here, the domains represent areas spontaneously magnetized up to saturation, which are separated from each other by the so-called Bloch walls [3]. The alignment of the magnetization vectors of the domains is statistically distributed over a ferromagnetic sample in the non-magnetized state in such a way that their total effect is completely neutralized. The magnetic structure of iron-based ferromagnetic materials consists of two kinds of Bloch walls, 180° Bloch walls and 90° Bloch walls. The indicated angle represents the angle between the magnetization vectors in two neighboring domains. The 180° Bloch walls have short-range stress fields resulting in their strong interaction with microstructure inhomogeneity situated locally (dislocations or precipitates) or micro-residual stresses. The 90° Bloch walls have long-range stress fields that cause a strong interaction with microstructure heterogeneities stretched out over hundreds of microns and more (microstructure phases) or residual stresses of the second or first kind.

Under the influence of an external magnetic field, ferromagnetic materials align the magnetization vectors of the domains in the direction of the external magnetic field. The domains also change the structure under the influence of stresses. Known processes, Bloch wall movements and rotations of the domain magnetization vectors, cause these changes. The underlying effect is magnetostriction and the Villari effect. Magnetostriction describes the change in length of a ferromagnetic material during magnetization. A distinction is made between materials with positive and negative magnetostriction, depending on whether a sample lengthens or shortens in the field direction. The magnitude of the change in length depends on the direction of the magnetic field relative to the crystal axes. The Villari effect describes the reversal case that an elastic change in geometry causes a change in magnetization state. The cause of the effects lies in the spin-orbit coupling [4, 5].

2.1.2 Magnetic hysteresis

With an external alternating field magnetization of ferromagnetic materials, there is no clear correlation between the magnetic field strength H and the magnetic flux density B . This means that the magnetization of a ferromagnetic material depends not only on the external field strength (H) but also on the time course of the magnetization [4, 5]. If the magnetic field strength H is increased in a

non-magnetized ferromagnetic material, the magnetic flux density B increases in its surroundings. If the field strength is reduced to zero again, the magnetic flux density remains at a value unequal to zero. The ferromagnetic material retains some residual magnetism (remanence). With periodic magnetization, a ferromagnetic material reacts with a hysteretic relation of flux density B and magnetic field H (see **Figure 1**) [4, 5]. With continuous periodic magnetization, the hysteresis curve is traversed once with each magnetization period.

The reason for the occurrence of hysteretic behavior is the interaction of Bloch walls and microstructure. The Bloch wall motion is discontinuous throughout the magnetization process, as the Bloch walls are pinned by existing lattice defects, and each pinning has to be overcome by increasing applied magnetic field. Lattice defects in the microstructure such as grain boundaries, dislocations and precipitates represent energetic minima for the Bloch walls. This causes the Bloch walls to tear loose abruptly and move until a pinning site of higher strength is reached.

Stresses affect the magnetic hysteresis behavior of ferromagnetic materials. In magnetostrictively positive materials (such as most ferromagnetic steels), tensile stress causes an increase of the differential susceptibility and a narrower hysteresis (H_C shift toward smaller values) and vice versa for compressive stresses. Magnetostrictively negative materials behave contrary to positive materials [4, 5, 7].

2.1.3 Magnetic Barkhausen noise

The analysis of magnetic Barkhausen noise (MBN) is based on a discovery by Barkhausen [8]: Abrupt changes in local magnetization caused by the discontinuous Bloch wall motion can be picked up inductively as a series of voltage pulses (noise) induced into a coil that is placed close to the material surface. The location of the highest density of these impulses is in relation to the magnetic hysteresis near the coercive force H_C , since this is where most Bloch wall jumps occur. The voltage pulses can be amplified, filtered and rectified for evaluation. The envelope of the filtered and rectified noise signal can be recorded as a function of the magnetization field strength, resulting in a so-called Barkhausen noise profile curve $M(H)$ (see **Figure 2**). The magnetic Barkhausen noise has a characteristic dependence on

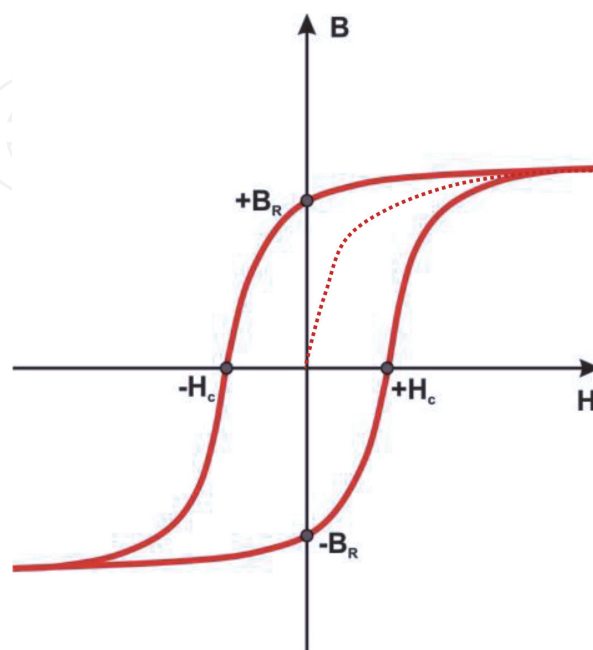


Figure 1.
Hysteresis curve (H_C , coercivity; B_R , remanence) [6].

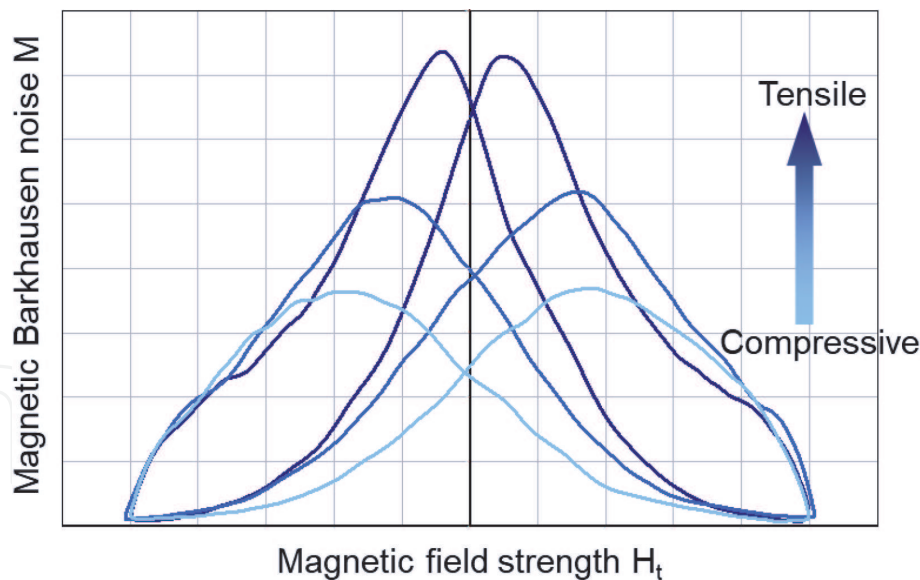


Figure 2. *Stress dependence of the magnetic Barkhausen noise profile curve for a single ferromagnetic sample in a tensile/compressive test in elastic strain range, without a change in the mechanical hardness (after [9]).*

mechanical stresses (see **Figure 2**), which makes it suitable for the nondestructive determination of residual stresses.

2.1.4 Micromagnetic multiparameter microstructure and stress analysis (3MA)

Micromagnetic multiparameter microstructure and stress analysis (3MA), developed at the Fraunhofer IZFP, is a solution for the quantitative determination of quality-deciding target parameters such as stress as well as hardness, hardening depth (CHD, SHD or NHD), ductile-to-brittle transition temperature (DBTT), yield and ultimate strength. 3MA uses a combination of several micromagnetic measuring methods such as upper harmonic analysis, Barkhausen noise analysis, incremental permeability analysis and eddy current (EC) impedance analysis [10]. The reason for using more than one measuring method for material characterization is the increased robustness against disturbing influences such as material inhomogeneity or surface treatment (similar to the benefits of having different human senses). The 3MA device generates the drive voltages for the magnetization coil and the eddy current coil in the sensor. The 3MA sensor includes an electromagnet, which excites an alternating magnetic field in the ferromagnetic sample, which, in turn, shows micromagnetic effects (see Section 2.1.2). In the most widespread implementation of 3MA, these effects are registered with a Hall probe and coils included in the sensor as well. Other implementations evaluate the current and voltage at the exciter coil. After preamplification, the measured signals are processed in the 3MA device and a controlling PC. This results in a kind of “magnetic fingerprint” which is used for quantitative and qualitative material characterization. For mechanical-technological material characterization, 3MA has to be calibrated on a well-defined calibration set of samples (with known target properties, e.g., stress or hardness).

2.2 Ultrasonic techniques

Among nondestructive methods, ultrasonic methods are the most and widely used ones. Reasons for this are the applicability to almost all materials and the wide range of wall thicknesses that can be tested. In order to excite ultrasonic waves, two main principles are used. Conventional ultrasonic testing is based on the use of the

inverse piezoelectric effect: an electrical voltage is applied to a solid (in this case usually ceramics) which leads to a deformation of the material and an excitation of ultrasonic waves. The (direct) piezoelectric effect is used to receive ultrasonic waves. In order to transfer the ultrasound into the specimen (and to receive it), a couplant is needed. In this regard, mostly water and oil are used. Depending on the situation, this implies disadvantages, such as a contamination of the specimen by the couplant and the limited excitation of wave modes. Nevertheless, piezoelectric ultrasound is widely used as a wide range of frequencies can be generated [11]. Electromagnetically excited ultrasound presents an advantageous alternative to conventional ultrasound testing, especially in rough environments or when special wave modes are to be excited. In principle, an electromagnetic acoustic transducer (EMAT) is consisting of a magnet and a radio frequency coil. The ultrasonic sources are induced in the material surface by alternating electromagnetic fields. Thus, on the one hand, no couplant is needed, and small lift-offs between specimen and transducers are acceptable. On the other hand, electromagnetic ultrasound can only be excited in electrically conductive materials, and the range of frequencies that can be generated is limited [12].

In order to perform measurements, regardless of the excitation mode, transducers are required to send and to receive ultrasonic waves. In this regard, different set-ups are feasible. **Figure 3** shows three typical set-ups that are used to measure the so-called ultrasonic time of flight (TOF), which denotes the time the wave (white) propagates from a transmitter (T) through a medium (green) to a receiver (R). Using reflection mode (see **Figure 3**, middle), generally, a transducer is chosen that serves as transmitter and receiver, and the generated wave is reflected at a medium boundary before it propagates back to the receiver. In addition to the TOF, the amplitude of the transmitted or reflected signal is recorded. If the thickness of the specimen is known, it is also possible to measure the velocity of propagation.

In addition to the ability to detect flaws, cracks, etc., ultrasonic techniques are often used to determine stresses. Reason for this is that all tension and strain changes in materials are subject to the so-called acousto-elastic effect which raises measurable changes regarding the velocity of propagation of ultrasonic waves [13]. Hence, measurements of ultrasonic velocity of propagation are used to detect emerging material and stress changes. Depending on the applied wave modes (longitudinal, transverse (SH, SV)) and their propagation and polarization direction in relation to the stress direction, additional changes of the measured ultrasonic TOF occur (**Figure 4**). The accuracy of evaluated stresses using ultrasonic TOF measurements is mainly determined by two factors, that is, the accuracy of the determined acousto-elastic constants and the accuracy of the measured TOF. According to [14] typical TOF measurements lead to an accuracy in the stress determination of

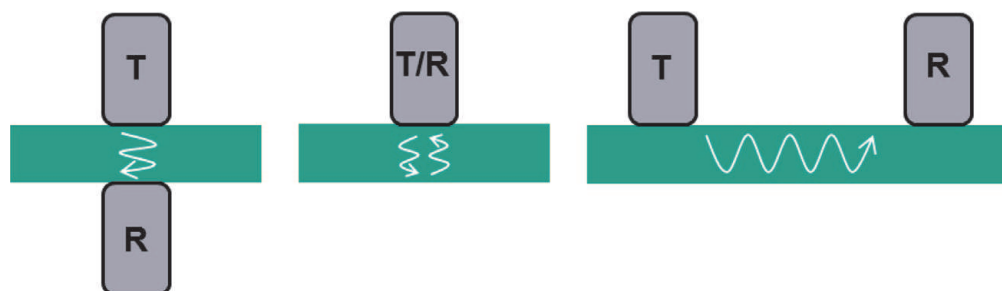


Figure 3. Three typical set-ups to perform ultrasonic measurements: T denotes the transmitter and R denotes the receiver, and the specimen is marked in green. Left, transmission mode; middle, reflection mode; right, transmission mode.

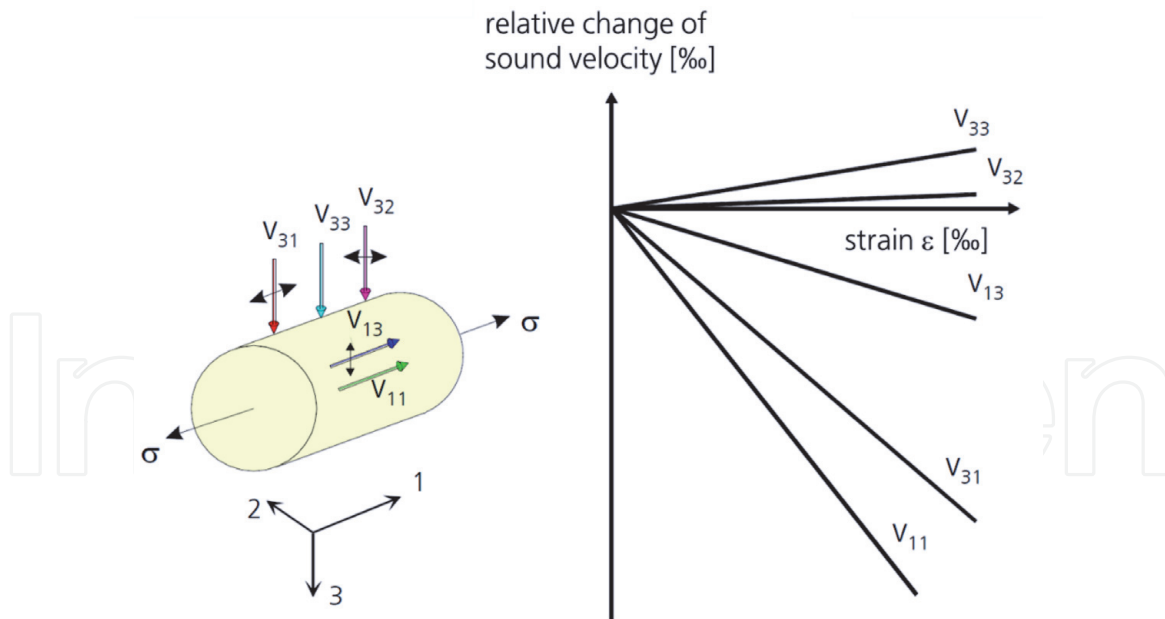


Figure 4. Relative change in the ultrasound velocity with the elastic tensile strain of a metallic sample: Schematic sketch (after [13]).

approx. ± 20 – 50 MPa. In order to measure a change of approx. 1% in the TOF, a stress change of approx. 100 MPa is needed. This, however, can only be understood as a rule of thumb as it strongly depends on the used wave mode and the material to be characterized. Measurements of steel rolls showed that longitudinal waves are more sensitive to stress changes than transversal waves: while a change in the stress state of 135 MPa caused a change of 1% in the TOF of the used transversal wave, a change in the stress state of only 87 MPa caused a change of 1% in the TOF of the used longitudinal wave [14].

3. Micro- and macro-residual stresses

Looking into publications accepted by most researchers and engineers, residual stresses are categorized according to the length scale. In this context, a simple classification categorizes residual stresses into macro- and micro-residual stress [15, 16]. Macroscopic residual stresses are stress distributions whose range is several orders of magnitude greater than the microstructure of the material. This type of residual stresses originates, for example, from shot peening, bending, welding and cold hole punching. Microscopic residual stresses, on the other hand, are based on microstructural misfits between phase constituents and grains which can occur as a side effect of phase transformation, intergranular stresses and plastic deformation, for example [17].

According to [2, 15, 18, 19], residual stresses may be distinguished more precisely. The first type or first kind (σ_R^I) is the equivalent of macro-residual stresses—the volume average stresses—which has a range of some millimeters. The second type or second kind (σ_R^{II}) analog to micro-residual stresses results from the heterogeneity of grains in polycrystalline materials and is defined as the mean stress value equilibrated inside a grain. The third kind (σ_R^{III}) as (sub)micro-residual stress contains all stresses at any point inside a grain which equilibrate on a scale of several atoms [18–20]. **Figure 5** shows a schematic summary of the three kinds of stresses.

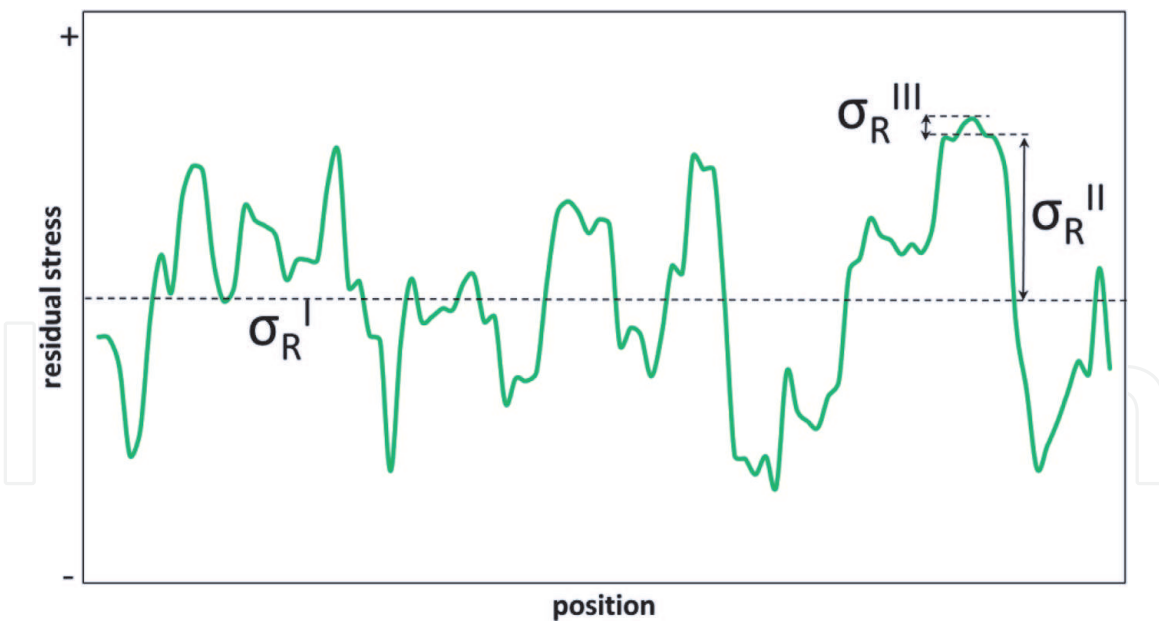


Figure 5. Three kinds of residual stress over several grains: σ_R^I represents the average stress over a longer range, that is, across several grains, σ_R^{II} represents a shorter-range average (i.e., representing one grain or crystal), and σ_R^{III} represents stress variations within a grain (after [15]).

3.1 Characterization of macro-residual stress

3.1.1 Characterization of macro-residual stress by means of micromagnetic techniques

In the frame of a research project funded by the German Research Foundation (DFG), the residual stress distribution in deep drawn components was examined by means of the micromagnetic method 3MA [9], which is described in Section 2.1.4. The focus of this research project was the examination of high-strength steels in deep drawing, which are increasingly used within the construction of automotive parts due to the reduction of weight with simultaneous enhancement of safety. The reduction of weight is an important contribution to the reduction of primary energy consumption in transportation and so finally adds a contribution to the reduction of CO₂ emissions. However, the application of high-strength steels in deep drawing processes is related to an increase of spring-back. Spring-back is one important criteria for accuracy of the shape geometry. One reason for spring-back is the redistribution of residual stresses when the part is taken from the forming tool [21]. On the other side, the material properties and the deep drawing process parameters are also influencing the spring-back behavior [22]. One aim of the abovementioned project was the determination of the residual stress and its distribution in the deep drawing components with the target to control the process parameters in order to avoid spring-back. The following example demonstrates the correlation between residual stress and spring-back and the potential of the micromagnetic 3MA method for the nondestructive characterization of stress states.

In order to investigate the influence of stress and strain during the deep drawing process on spring-back, six samples with three different rectangular geometries (160 mm × 80 mm), as shown in **Figure 6**, were produced. The three geometries are:

- Rectangular geometry
- Rectangular geometry, trimmed on the small sides of the part in order to remove the influence of the corners on the sample (decreasing stiffness)

- U-shaped geometry

For each geometry, a twin sample was provided.

The 3MA probe was manually and step vice moved along a measuring trace from the middle of the bottom (position 0 according to **Figure 7**) along the wall to the die radius (position 8 according to **Figure 7**). Hereby the samples have been magnetized parallel to the die (or punch) radius by using a magnetization frequency of 250 Hz and a magnetization field strength of 10 A/cm. For each measuring position, 41 measuring parameters derived from upper harmonic analysis, Barkhausen noise analysis, incremental permeability analysis and eddy current impedance analysis were recorded.

For a quantitative determination of residual stress, a calibration procedure is necessary. For the calibration, generally the micromagnetic measuring parameters are correlated to real stress values at a corresponding position, which are measured by a reference method. Bases on these calibration data, a numerical function is generated, which is able to calculate stress values out of the micromagnetic measuring parameters. For the calibration of the shown example, the Barkhausen noise values which yielded the best results out of all the 3MA values were correlated with the tangential component of the residual stress values measured by X-ray diffractometer (XRD). As the samples have been magnetized parallel to the die (or punch), the magnetic measurements are mostly sensitive to the tangential component of the residual stress.

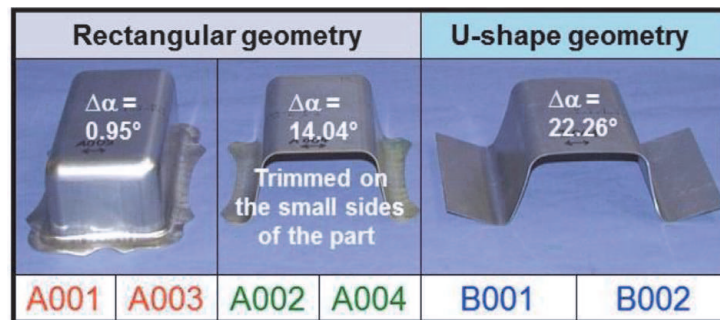


Figure 6. Examined shapes and correlated spring-back angle $\Delta\alpha$ (two samples for each shape). The labels below the photos relate to the legend in **Figure 7** [9].

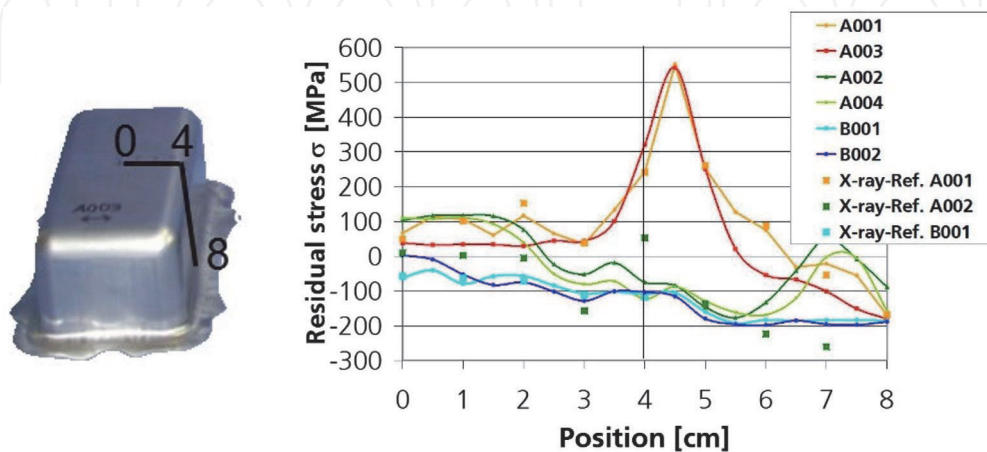


Figure 7. Residual stress distribution determined micromagnetically by 3MA on a rectangular geometry (A001, A003), a rectangular geometry trimmed on the small sides of the part (A002, A004) and a U-shaped geometry (B001, B002) along a measuring trace from the center of the part bottom (position 0) down to the die radius (position 8) [9].

The graph in **Figure 7** shows the behavior of the micromagnetically determined residual stress on a rectangular geometry, a rectangular geometry trimmed on the small sides of the part and a U-shaped geometry. In the range between positions 4 and 5 cm, a decisive decrease of tensile residual stresses after cutting free is observed. Due to the cutting process and the resulting relief of tensile residual stress, the deep drawn part shows a clear spring-back and hence an increase of the spring-back angle $\Delta\alpha$. The U-shaped sample shows a quite homogenous distribution of stress in a low level along the measured line. Due to the missing sidewall, the sample can expand when taken out from the deep drawing tool, and therefore the spring-back angle increases, and the stress level stays small.

3.1.2 Characterization of macro-residual stress by means of ultrasonic techniques

In this paragraph, a study regarding integral biaxial stress conditions at rolled aluminum sheets for a stretched (0.5%) and an unstretched condition is presented and discussed in order to show the influence of the stretching process on residual stress relief. As for aluminum, the ultrasound velocity is almost equally affected by rolling texture and stress of the material—whereas for steels the ultrasound velocity is affected approximately 10 times more due to the rolling texture compared to stress conditions—these effects need to be separated from each other to determine the existing stress states.

Under the assumption that the stress component along the thickness direction can be neglected due to the texture, the two principal stress directions in and perpendicular to the rolling direction can be determined having information of two directional TOF dependencies. In order to easily implement measurements, an EMAT in impulse-echo mode (cf. **Figure 3** middle) using a center frequency of 2.5 MHz, three bursts and a bandpass filter generating ultrasonic shear waves propagating across the thickness of the sheets, polarized in and perpendicular to the rolling direction by turning the transducer around its own axis at each measuring point, were applied.

Figure 8 shows the distribution of the measured relative TOF changes of the two polarized shear waves due to the two principal stress directions (in and perpendicular to the rolling direction) concerning the formula

$$\text{Relative TOF [\%]} = \frac{\text{TOF in rollingdirection} - \text{TOF perpendicular to the rolling direction}}{\text{TOF perpendicular to the rolling direction}} \times 1000 \quad (1)$$

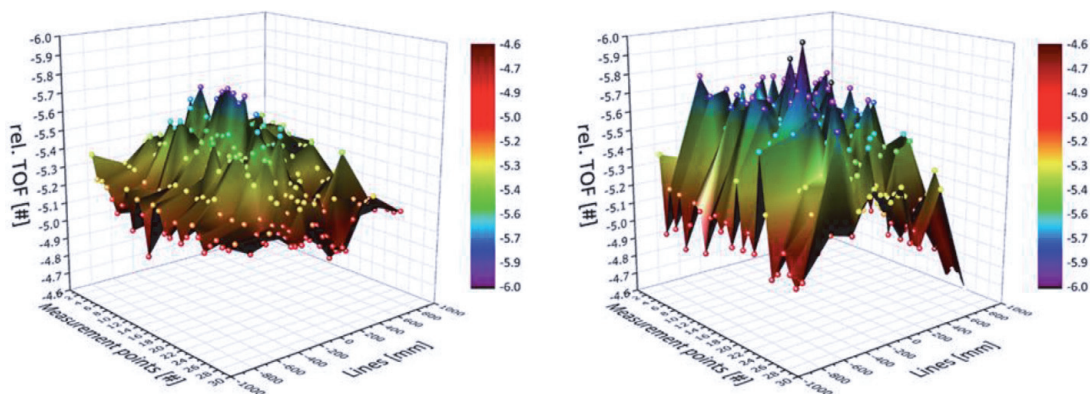


Figure 8.
 Distribution of relative TOF measurements at a stretched (0.5%) sheet (left) and an unstretched sheet (right).

at 297 measuring points at a stretched (left) and an unstretched sheet (right) of 30 mm thickness and a flat profile of 2 m × 4 m.

In both diagrams displayed in **Figure 8**, the superimposed influence of the rolling texture and the residual stress state is contained in each measurement point. In order to separate them from each other, the texture needs to be determined by measurements at selected measuring points that have to be cut out in order to relieve the stress condition or at a comparative sample of the same microstructure in a stress-relief heat-treated condition. Afterwards, quantitative stress values can be calculated using the TOF values and the acousto-elastic constants evaluated in tensile tests [13]. Under the assumption of an even distribution of the texture due to the rolling process, the shapes of the measurement results of **Figure 8** reflect the residual stress distribution for the stretched (0.5%) and the unstretched sheet originating from the two principal stress directions.

3.1.2.1 Evaluation of absolute stress in the two principal stress directions for platelike products

For the determination of individual values of two principal stress components at sheets, an additional information concerning the local thickness of the sheets is necessary compared to the approach mentioned above. The principle described in this paragraph can, therefore, be applied using a newly developed hybrid EMAT.

Due to the excitation mechanism, the hybrid EMAT is linked conductively to non-ferromagnetic materials. This kind of EMAT generates two different ultrasonic waves in a time multiplex at the same measurement point. On the one hand, a shear wave propagating across the thickness of the sheet oscillating perpendicular to its direction of propagation is generated, and on the other hand, a longitudinal wave propagating across the thickness oscillating in the same direction is generated.

Depending on the position of the transducer, the anisotropy of the shear wave velocity can be evaluated by turning the transducer around its axis. Since the TOF of the longitudinal wave is not affected by any stress condition across the thickness of the sheet, there is no significant anisotropy for this wave type. Thereafter, reliable information on the thickness of the sheet can be obtained at each measurement point.

Using the evaluated thickness for a stress-free state determined by the longitudinal wave and information on the anisotropy of the two shear waves oscillating in and perpendicular to the rolling direction, the shear wave velocities can be determined. Afterwards, the two main stress states V_{ij} and V_{ik} can be calculated according to Eqs. (3) and (4) below, using the shear wave velocities evaluated previously.

$$\frac{v_{ii} - v_L}{v_L} = \frac{A}{C} \cdot \sigma_i + \frac{B}{C} \cdot (\sigma_j + \sigma_k) \quad (2)$$

$$\frac{v_{ij} - v_T}{v_T} = \frac{D}{K} \cdot \sigma_i + \frac{H}{K} \cdot \sigma_j + \frac{F}{K} \cdot \sigma_k \quad (3)$$

$$\frac{v_{ik} - v_T}{v_T} = \frac{D}{K} \cdot \sigma_i + \frac{F}{K} \cdot \sigma_j + \frac{H}{K} \cdot \sigma_k \quad (4)$$

In Eqs. (2)–(4), σ_i , σ_j and σ_k represent the components of a normalized stress tensor, and v_L and v_T define the ultrasound velocity of a longitudinal (L) and transverse (T) wave for a stress-free condition. v (with its two indices) denotes the ultrasonic velocity for different directions of propagation (first index) and oscillation (second index) for a stress-affected state. A, B, C, D, H, F and K are

combinations of the second- and the third-order elastic constants, the quotients of which define weighting factors for the corresponding main stress directions [13].

3.1.2.2 Depth-resolved measurements

Following, an innovative approach is described in order to determine depth-resolved stress conditions using EMATs generating Rayleigh waves in transmission mode in ferromagnetic or conductive materials.

A smart layout of the transducers offers the opportunity to generate and receive Rayleigh waves operating at different frequencies in a time multiplex using the same transducers. The general EMAT concept is explained for ferromagnetic materials here, but it can be applied to non-ferromagnetic ones as well, by modifying the transducer set-up. It is based on the superposition of a perpendicular bias magnetic field B_0 and a high-frequency field generated by a meander-shaped coil that is wound on the ferromagnetic comb structure (**Figure 9**). The generated trace wavelength, λ_s , is defined as the distance of two neighboring wires wound into the grooves of the comb having the same current direction. By winding the coil on just every second or third tooth, respectively, by segmenting the coil into several single coils for each comb tooth using an additionally adequate electrical connecting, the trace wavelength can be varied (λ_{s1} , λ_{s2} , λ_{s3}).

As the penetration depth of a Rayleigh wave is approximately in the range of one wavelength [24], different depth ranges can be achieved. Approaching specific evaluation algorithms comparable to the one mentioned in [25], stress conditions in different depths can be resolved. Since the stress dependence of the ultrasound velocity of a Rayleigh wave is less than for longitudinal and transversal wave types due to the elliptic polarization, the stress resolution is comparatively small.

3.1.2.3 Ultrasonic determination of residual stress and the separation from texture effects on AHSS strips

Advanced high-strength steel (AHSS) enables the automotive industry to increase the stability and crash safety of cars and to reduce weight or CO₂ emissions at the same time. Increasing strip speeds and requirements on the lateral homogeneity of the material properties leads to a need for a development of a nondestructive multisensor solution for the quality assurance. The homogeneity of the texture, grain size and the influence of residual stresses in the material is of great importance for the deformation behavior and decisive for material processing, such as deep drawing or welding. Current in-line NDT systems determine only a subset of the required parameters and do not assess their homogeneity across the strip width.

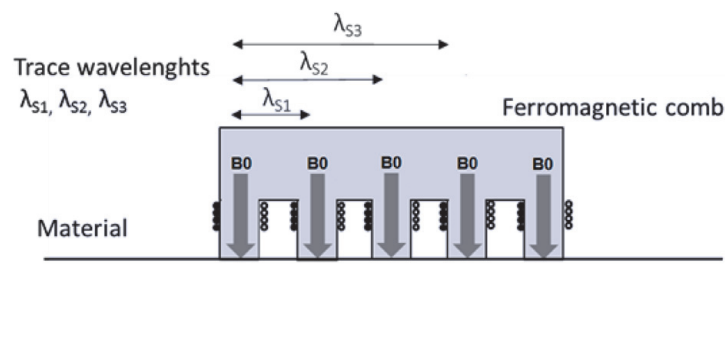


Figure 9. Set-up of an electromagnetic acoustic Rayleigh wave transducer for generating variable trace wavelengths (after [23]).

In this context, Fraunhofer IZFP developed a hybrid test system for the in-line inspection of AHSS consisting of 3MA and ultrasonic TOF measurements using EMAT.

The challenge in the case of the ultrasonic inspection is the separation of the different effects from texture and residual stresses on the ultrasonic time of flight. The impact on the ultrasonic wave velocity is ranging in a magnitude of percentage to per mil. The objective of the new approach is the use of different wave modes and types to separate the effects. In thin plates, guided waves can be excited with EMAT. By different alignments of the conductive paths to the magnetic field in EMAT, a simultaneous excitation of guided shear horizontal (SH) waves and Lamb waves is possible. Selecting different excitation frequencies and switching between symmetric and antisymmetric modes of different order could be realized.

Because of its symmetry to the texture direction, the lowest symmetric mode of the SH wave (SH_0) could be used to determine the residual stress. The time-of-flight measurement of this wave mode in rolling direction (0°) and perpendicular to it (90°) is therefore independent of the influence of texture. The presence of residual stress is reflected in an asymmetrical behavior in the polar plot (see **Figure 10**). Additionally, the SH_0 mode is dispersion-free and thus independent of thickness, which means that even slight fluctuations in sheet thickness have no influence on the measuring effect.

If the influence of the residual stress is known, the effect can also be calculated for the other wave modes and types, and finally the influence of texture can be determined.

In order to implement the inspection concept, a special arrangement of the probes is required (see **Figure 10**). Thus, the macro-residual stress is determined as an integral value over the sheet thickness and the travel distance of the wave.

3.1.2.4 Residual stress analysis in freight car wheels and research challenges of localized stress evaluation

Residual stress occurring during operation of components can also be detected and quantified with ultrasonic methods. The examination of residual stress in railway wheels of freight cars is an industrial application of ultrasonic stress evaluation that has been established more than 25 years ago [27]. In the production of new wheels, compressive stresses in the tread in the circumferential direction are generated by well-defined quenching, which should prevent the formation of cracks in the wheel-rail contact zone in case of damage to the surface. However, in the case of block-braked freight car wheels, the running surface is subjected to high

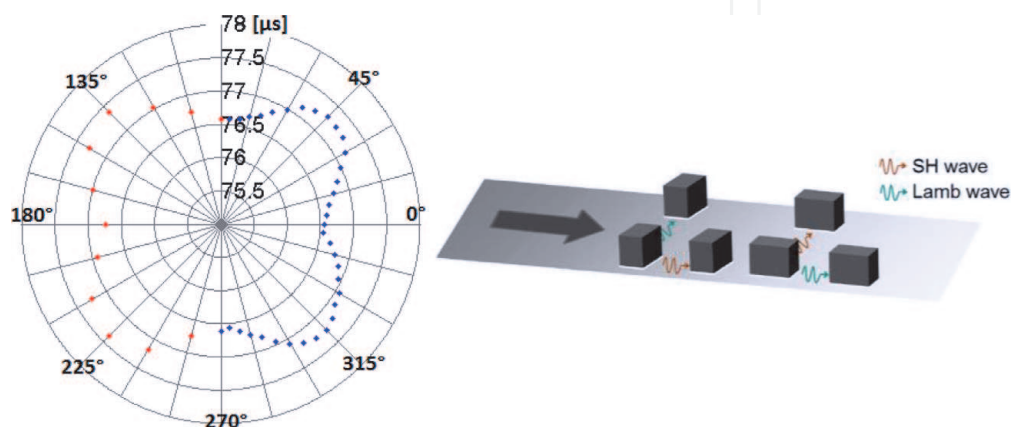


Figure 10. Time of flight of SH_0 mode depending on the rotation angle, measured on an AHSS plate (left). Arrangement of probes along the steel strip (right, after [26]).

thermomechanical loads, which, depending on the axle load and the route profile, lead to high energy input in the form of heat. In addition, faulty, non-opening brakes cause the material to overheat, which, in turn, results in compressive stress being converted into tensile stress that may increase until rim failure occurs. There are various systems that determine these stress values in the industrial environment by means of ultrasonic methods. The procedures and evaluation steps presented here refer to the only system for the fully automatic determination of circumferential residual stresses. This system represents a development of Fraunhofer IZFP and has been used for more than 25 years in maintenance and wheel production, presently in the fourth generation.

In order to check the wheel for critical stress situations, the acoustic birefringence parallel to the tread is evaluated from the side of the wheel rim. For this task, a linearly polarized shear wave is used, since this wave type exhibits the strongest interaction with the stress in the circumferential direction for the given geometry. The required ultrasonic wave is generated with an EMAT that excites the wave in the ferromagnetic base material of the wheel without a coupling agent (**Figure 11**). Also due to the geometry and surface condition of used wheels, only the relative stress difference with respect to the radial direction of the wheel rim is checked. A measurement of the absolute change in the sound velocity is not possible within the scope of the required accuracy of the sound path determination in the maintenance of the track wheels.

When determining the relative stress difference, the measurement of the ultrasonic time of flight of the linearly polarized wave with its direction of oscillation perpendicular to the running surface is chosen as reference, as the stresses in the radial direction do not change over the life of the wheel according to experience. The test as well as the presentation of the results takes place as a depth profile of the tread in the direction of the wheel web. The typical step size of the measurement is 1 mm. **Figure 11** shows the test positions and the wave propagation of the ultrasound schematically.

Since the acousto-elastic material constant K is known, the measured differences in the ultrasonic time of flight of the two measuring tracks can be converted into a relative stress value between the tangential and the radial direction of the wheel. This is done at each test position according to Eq. (5):

$$\sigma_{tan} - \sigma_{rad} = K \frac{TOF_{tan} - TOF_{rad}}{TOF_{rad}} \quad (5)$$

The result is a stress curve in the depth direction. Each stress value represents an integral result over the entire traveled sound path, as shown in **Figure 12**. Depending on whether a newly manufactured wheel or the review of a used wheel

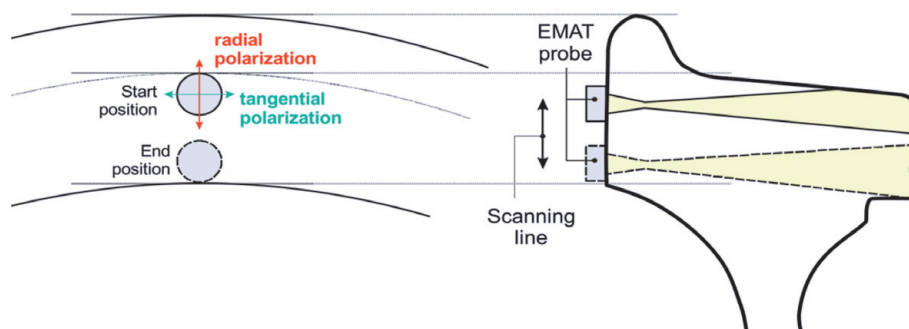


Figure 11. Principle of the stress evaluation of the railroad wheel. The scan is performed in steps of 1 mm. The EMAT transceiver with the probe generates a linear polarized shear wave.

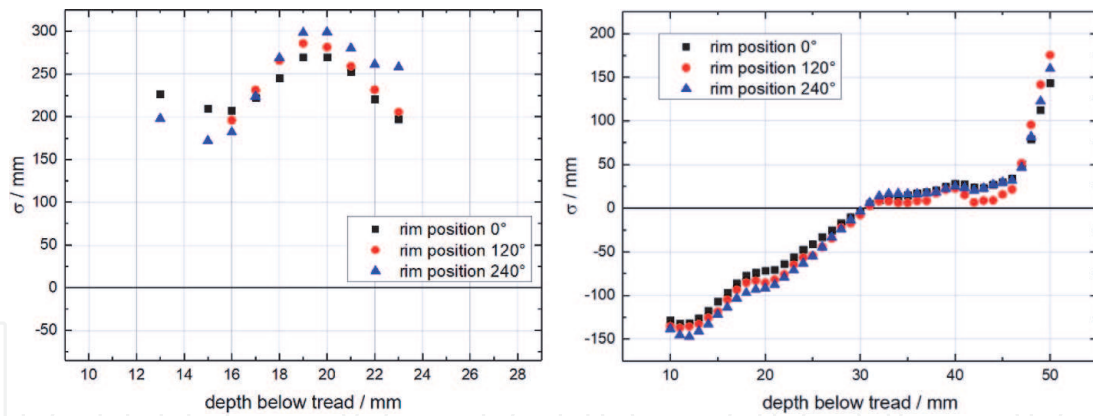


Figure 12. Typical stress graph of a “R7” wheel in new condition (left) and another wheel of this type in worn and used condition. In each case, tests were performed on each wheel on three positions with an offset by 120°.

is required, different stress limits were applied, which decide on the further operation of the freight car wheel. **Figure 12** shows a comparison between the residual stress of a new and a used wheel.

Now, block-braked track wheels are experiencing a recurrence, also in passenger transport, as a result of which the wheel developers’ desire for improved methods for determining local residual stress is emerging. By fundamentally linking finite element computation and knowledge of ultrasonic wave interactions with sample volume stresses, geometrical and thermomechanical states can be predicted. These predictions represent possible solutions for real stress situations leading to the measured integral stresses. Modeling to predict possible wheel residual stress as a first step is a well-known method [28]. The challenges, however, lie in the combination with sufficiently large amounts of residual integral residual stress data as well as the real geometries investigated. With the help of this data, test systems would be able to identify most likely the stress distribution depending on the wheel geometry, which leads to the present measurement result, and thus to make statements about critical local stresses along the sound propagation path.

This procedure for combining preliminary information as a statistical interpretation aid for metrologically inaccessible information beyond the described application is a research field with high potential for improvements in the informational quality of volumetric residual stress evaluation.

3.2 Characterization of micro-residual stress

3.2.1 Characterization of micro-residual stress by means of micromagnetic techniques

3.2.1.1 Volumetric characterization

Micromagnetic testing methods are based on the fact that the ferromagnetic material behavior is influenced by microstructures as well as by applied load or residual stress. Separation of these two influences in micromagnetics can be carried out by analyzing different interaction mechanisms of magnetic structure with microstructure, on the one hand, and with residual or applied stresses, on the other hand. Moreover, it is well-known that microstructure changes always cause changes in the micro-residual stress distribution. This means that, in fact, separating micro-residual stress from macro-residual or load stress indirectly allows for the separation of microstructure from macro-residual stress.

Therefore, a nondestructive micromagnetic testing approach has been developed for the evaluation of material changes independently on the macro-residual

stresses [29]. This approach is based on the applied stress dependence of signals obtained from magnetic hysteresis loop at different applied load stresses in the elastic range. The magnetic hysteresis curve changes its shape under influence of applied load stresses depending on whether the applied load stresses are compressive or tensile. It has been observed experimentally that magnetic hysteresis curves recorded at different applied load stresses contain two intersection points that are invariant with changing applied stress. A possible explanation of this effect is that the magnetization processes at these points take place by 180° Bloch wall movements only. 180° Bloch walls have short-range stress fields, whereas 90° Bloch walls have long-range stress fields. As the intersection points do not change their position with changing applied stress, they are stress-independent, and therefore the magnetization processes in these points are based on 180° Bloch wall movements only. Parameters that define these intersection points are the related magnetic field strength H_{sp} and flux density B_{sp} (Figure 13). This means that both parameters H_{sp} and B_{sp} characterize the 180° Bloch wall movement only and are affected by short-range residual stresses or microstructure features that can induce them. Microstructure defects, e.g., second-phase precipitates, or dislocations induce such short-range residual stresses.

Furthermore, micromagnetic measurements have been carried out on cylindrical specimens of 20MnMoNi5-5 steel at superimposed elastic compressive and tensile load stress in the range of -150 MPa up to 200 MPa, and the stress invariant points have been determined automatically. In the first step, stress invariant points were determined on stress-relieved specimens of different microstructures with different mechanical properties. X-ray measurements confirmed that the samples were nearly free from residual stress (the maximum stress observed was 50 MPa). It was found that parameter H_{sp} depends almost linearly on the yield strength values of those samples (Figure 14). In order to induce microstructure changes, the samples have been plastically deformed to 1 and 2% plastic deformation. After each plastic deformation the samples have been investigated by means of the approach described above. It has been observed that the increase of the plastic deformation leads to an increase of H_{sp} . The change of H_{sp} with increasing plastic deformation depends on the initial mechanical properties of the samples. In the case of the samples with high yield strength, H_{sp} increased almost linearly with the percentage

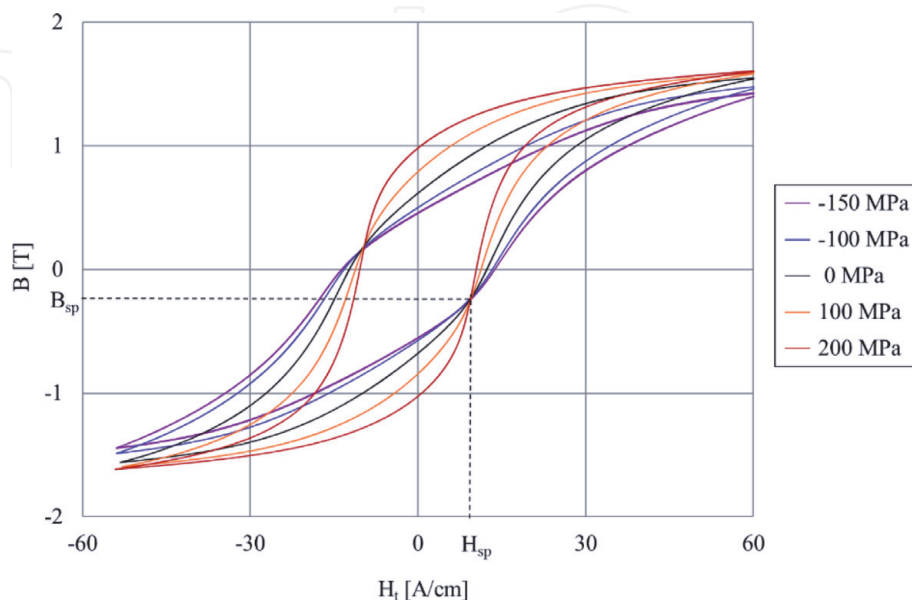


Figure 13. Hysteresis curves measured as different superimposed load stress levels including the invariant stress points and their corresponding coordinates (after [29]).

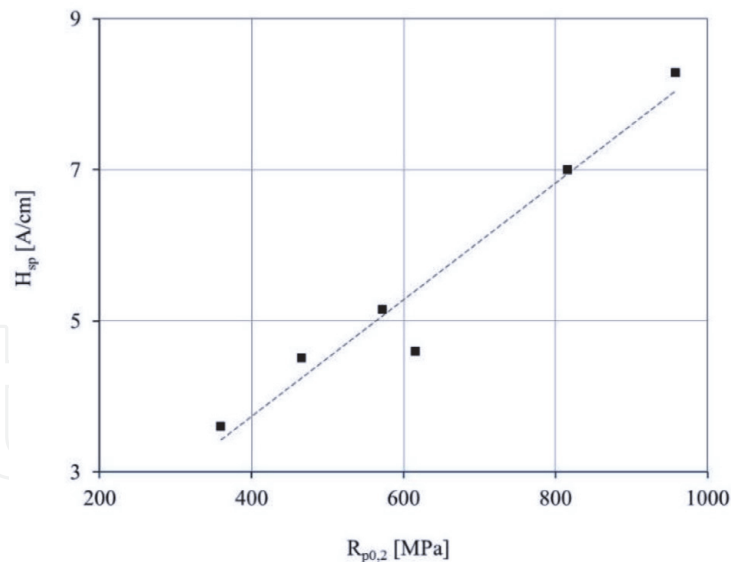


Figure 14.
Dependency of parameter H_{sp} on the yield strength $R_{p0.2}$ (after [29]).

of plastic deformation. In the case of the sample with low yield strength, H_{sp} does not change, whereas in the case of the samples with average yield strength, H_{sp} changed up to 1% of plastic deformation and after that remained constant. In the case of soft materials, the dislocation density changes only after higher degrees of plastic deformation. The more mechanically soft a material is, the more malleable it is, due to the absence of microstructure defects. Due to this fact, in the case of mechanically soft microstructures, H_{sp} remains constant for plastic deformation degrees $\leq 2\%$ and would probably increase at higher plastic deformation degrees. With increasing yield strength (mechanical hardness), the ductility of the materials decreases, and the dislocation density already takes place at smaller plastic deformation degrees. For this reason, H_{sp} increases in the case of mechanically hard microstructures even after a small plastic deformation ($< 1\%$).

Moreover, experiments have shown that for samples containing compressive residual stress, stress invariant points occur only when applying compressive stress, whereas for samples containing tensile residual stress, stress invariant points occur when applying either compressive or tensile stress. This means that the sign of applied stress (compressive or tensile) under which the stress invariant point occurs gives information on the sign of the residual stress in the sample.

In practice, this approach is applicable in the context of a monitoring concept if the operating conditions provide for or permit the variation of the operating pressure. A further possible application of this approach is the characterization of the microstructure in the frame of material development, for example, on a material containing macro tensile stress as a result of processing.

The procedure described above allows for the characterization of micro-residual stress induced by dislocations. Micromagnetic measurement techniques based on the tensile load-dependent maximum of the Barkhausen noise amplitude can be used for the analysis of micro (third kind)-residual stress. Such stresses can be induced, e.g., by nanoscale second-phase precipitates due to the difference in lattice parameters of Cu and Fe. For this purpose, Fe-Cu alloys with well-defined amounts of nanoscale Cu precipitates have been manufactured and investigated. The micromagnetic concept is based on load stress-dependent Barkhausen noise measurements. The maximum of the Barkhausen noise amplitude (M_{MAX}) obtained during one hysteresis cycle at a time is recorded under varied tensile load stresses, leading to an $M_{MAX}(\sigma)$ curve that has a relative maximum. A shift of this relative maximum along the stress axis can be observed as a measure for the change of the

micro- or macro-residual stress condition. A measurement technique based on this effect permits the quantitative characterization of residual stress variations without the use of a reference method such as X-ray diffraction. If the superimposed residual stress is of the tensile type, the Barkhausen noise activity of the iron-based materials is more enhanced than in the stress-free condition, and the curves reach their maximum at lower load stresses, that is, the curve shifts to the left-hand side and in the other direction in the case of superimposed compressive stress. In order to determine the micro-residual stresses induced by nanoscale Cu particles only (i.e., to eliminate the influence of macro-residual stress from quenching and micro-residual stress from different thermal expansion coefficients of particles and surrounding matrix), micromagnetic measurements have been performed in three steps, which are described in [30, 31]. This procedure permits the volumetric evaluation of micro-residual stresses.

3.2.1.2 Imaging of local residual stress distribution using Barkhausen noise and eddy current microscopy (BEMI)

The fundamental sensor principle of 3MA has been implemented in many technological variants and sizes, even down to where microscopic lateral resolution is reached: The Barkhausen noise and eddy current microscope (BEMI) is a scanning probe device based on miniature micromagnetic sensors [32]. So far, two sensor designs have been implemented as BEMI modules:

- *Ferrite core sensor:* Copper coils wound on a small ferritic core with a 300-nm-wide gap facing the sample surface are used for picking up magnetic Barkhausen noise (MBN) during cyclic magnetization of the sample, for characterizing permeability and conductivity in an eddy current (EC) operation mode and for measuring eddy current incremental permeability (ECIP). The MBN, EC and ECIP modes are performed alternately using a 3MA controller device. Depending on the material, a lateral resolution of about 10–20 μm is achieved [33].
- *Point probe:* A needle-shaped ferromagnetic core equipped with a primary (excitation) and a secondary (detection) coil is applied for characterizing local permeability and magnetic field [34]. The sample properties close to the needle tip strongly affect the secondary coil voltage waveform under application of sinusoidal voltage to the primary coil. Point probes deliver isotropic lateral response at a resolution depending on the sharpness of the needle tip. Experiments have proven that some features can be determined with a resolution of around 20 μm [35].

For both sensor types, an evaluation software determines the characteristic features from the signals received. As further explained in the previous sections of this contribution, magnetic Barkhausen noise amplitude and magnetic permeability are strongly modulated by local stress for a given material. This leads to a lateral stress-dependent contrast in feature images produced by BEMI. Multiple mathematical and procedural approaches are applied for predicting stress quantitatively in an indirect way, using these micromagnetic features as input.

On the example of locally laser-treated X20Cr13 steel, the stress sensitivity of features obtained with both probe types is demonstrated. The sample shown in **Figure 15(a)** was scanned with a point probe, **Figure 15(b)**, and ferrite core sensor, **Figure 15(c)**. The results, as shown in **Figure 16**, indicate strong stress fields surrounding the laser-treated spots. The actual stress values were determined with

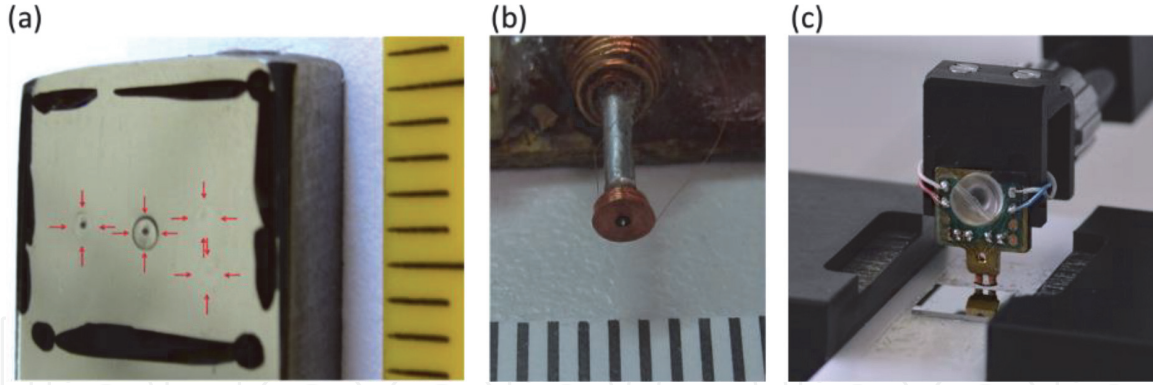


Figure 15. (a) Photo of X20Cr13 steel sample with laser-heated spots (scale unit is millimeters) [35]. (b) Photo of point probe [35]; (c) photo of ferrite core sensor (Fraunhofer IZFP).

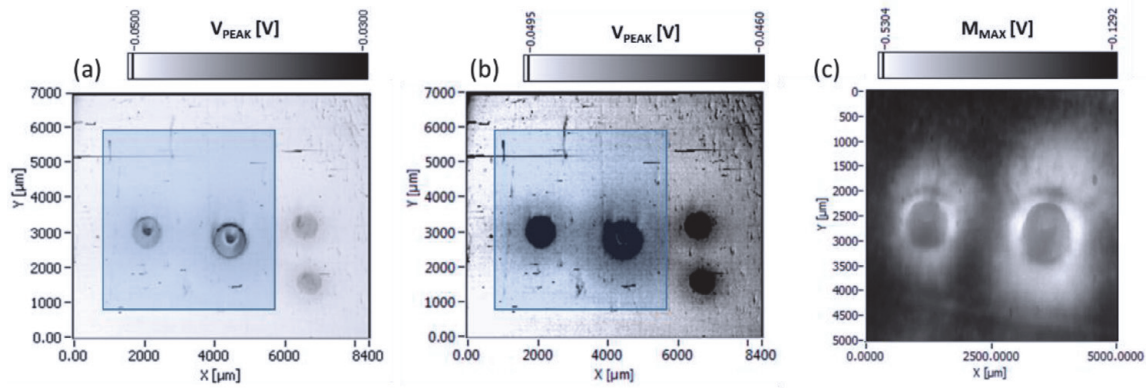


Figure 16. (a) Scan of point probe feature V_{PEAK} in the area marked in **Figure 15(a)**; (b) the same V_{PEAK} scan with narrow grey scale value range exposing stress fields around the laser-treated spots; (c) magnetic Barkhausen noise peak M_{MAX} of two laser-hardened spots inside the framed area [33, 35].

X-ray diffraction and indicated peak stresses M ranging from -300 MPa up to $+600$ MPa.

The novel micro-residual stress mapping method based on magnetic Barkhausen noise (RESTMAB) approach allows for a nondestructive estimation of micro-residual stress of ferromagnetic materials without any help from conventional stress measurement methods. Moreover, RESTMAB is a timesaving approach for quantitative stress determination with BEMI.

As previously mentioned, the position of the maximum of the $M_{MAX}(\sigma)$ curve is proportional to micro-residual stress (**Figure 17(a)**). As an example, the micro-residual stress inside a pre-deformed sample is calculated using Eq. (6):

$$\sigma_R = \sigma_{crit.(n)} - \sigma_{crit.(p)} \quad (6)$$

where σ_R is the residual stress and $\sigma_{crit.(n)}$ and $\sigma_{crit.(p)}$ are the applied stresses in the maximum of the $M_{MAX}(\sigma)$ curve for the non- and pre-deformed samples, respectively.

RESTMAB works based on the information extracted from the $M_{MAX}(\sigma)$ curve and using regression analysis for calibration. The residual stress and the M_{MAX} values are the inputs of the regression analysis. However, the $M_{MAX}(\sigma)$ curves require an adjustment prior to calibration. This adjustment is required because the MBN response is related to the sum of applied and residual stress. In other words, the MBN output shows the effect of residual stress and applied stress at the same time. Therefore, the M_{MAX} values in **Figure 17(a)** are affected by the residual and

applied stress, while the stress axis just presents the applied stress. As the separation of the effect of residual and applied stress for MBN is not possible, the stress axis is adjusted to show the sum of applied and residual stress. This is achieved by horizontally aligning the curves in their respective maxima. As shown in **Figure 17(b)**, the $M_{MAX}(\sigma)$ curves of the pre-deformed samples were moved to the $M_{MAX}(\sigma)$ curve of the non-deformed sample in such a way that all the maxima were aligned under the maximum of the $M_{MAX}(\sigma)$ curve of the non-deformed sample [20]. The residual stress σ_R of each sample is then measured based on the peak shift compared to this reference, using Eq. (7):

$$\sigma_{tot.} = \sigma_{app.} + \sigma_R \quad (7)$$

where $\sigma_{tot.}$, $\sigma_{app.}$, and σ_R are total, applied, and residual stresses, respectively. After modification of the stress axis, the modified stress and M_{MAX} parameters are used as input for a regression analysis in order to determine a polynomial expression for the relation between MBN parameters and (total) stress.

Figure 18 shows the $M_{MAX}(\sigma)$ curves before and after adjustment for non-deformed, 1 and 3% pre-deformed high-strength steel, respectively, and **Figure 19** shows the relation between measured and estimated stress after calibration. The measured stress values are obtained by the summation of the applied stress determined by the load cell of the tensile machine and the residual stress of the sample calculated by means of the shift between the peak positions at the $M_{MAX}(\sigma)$ curves (**Figure 18**). The estimated stress values show the residual stress calculated by means of the RESTMAB procedure.

Determination of the residual stress distribution in an arbitrary area with high lateral resolution is possible using BEMI calibrated with RESTMAB (**Figure 20**)

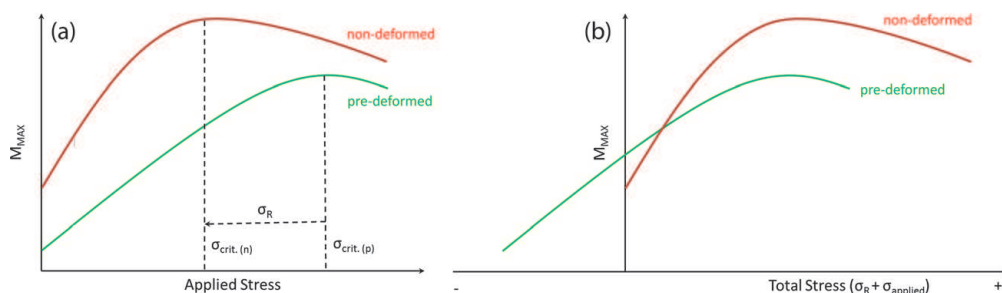


Figure 17. (a) Schematic $M_{MAX}(\sigma)$ curves for non- and pre-deformed material; (b) curves after horizontal alignment in the respective maxima [20].

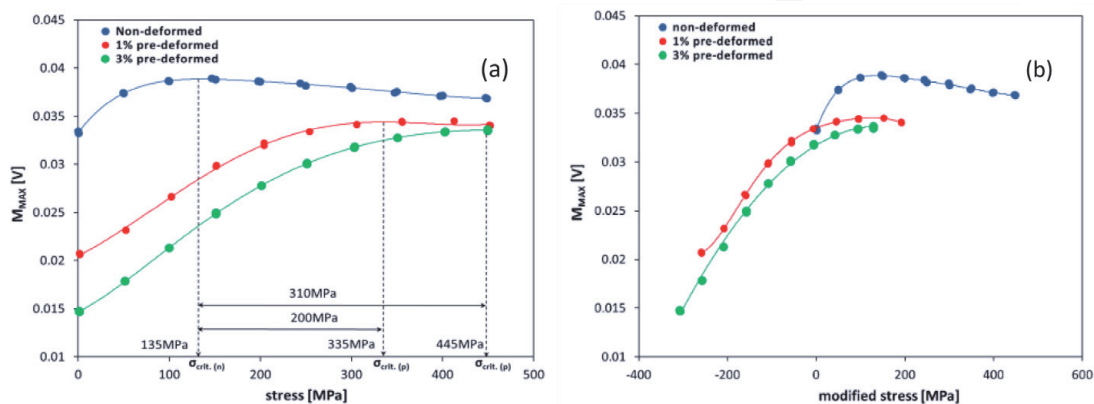


Figure 18. (a) Measured $M_{MAX}(\sigma)$ curves; (b) adjusted $M_{MAX}(\sigma)$ curves for the calibration process [20].

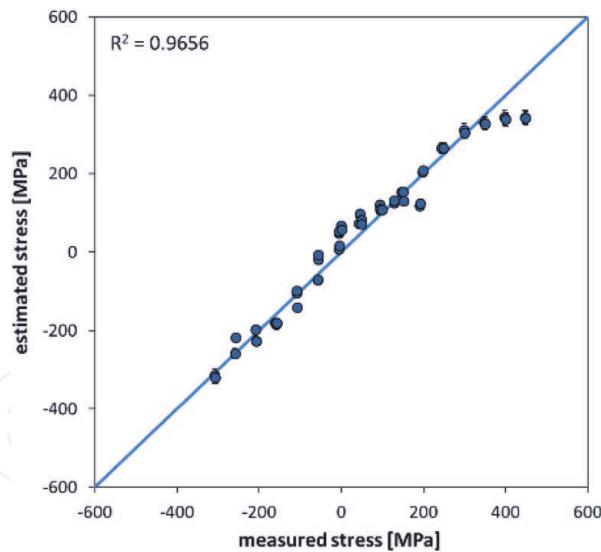


Figure 19. Relation between measured residual stress and estimated residual stress with RESTMAB for high-strength steel [20].

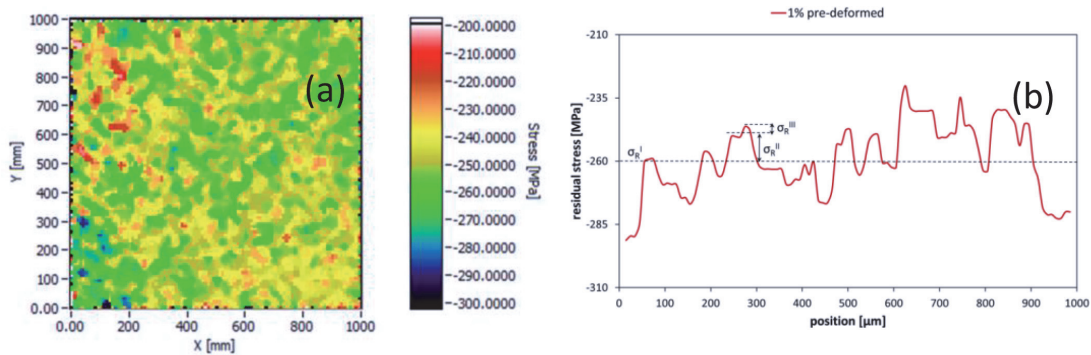


Figure 20. (a) Micro-residual stress distributions measured with the calibrated BEMI using the RESTMAB for 1% pre-deformed sample. (b) Line scan extracted from the scan, in which it shows different orders of residual stresses measured with the calibrated BEMI for high-strength steel [20].

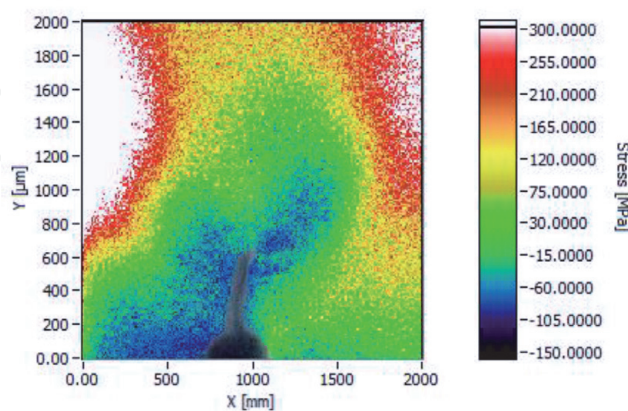


Figure 21. Residual stress distribution in front of a crack tip in high-strength steel using BEMI calibrated by means of RESTMAB. The overlaying sketch in dark gray shows the notch and crack [20].

illustrates the calibrated BEMI scan of pre-deformed sample of the high-strength steel, in which it shows the stress distributions of the sample in the scan area.

In another application, BEMI calibrated with RESTMAB was used to determine the stress distribution in front of a fatigue crack tip. **Figure 21** illustrates the stress

distribution as well as the plastic zone in front of a crack tip. Similar BEMI scans of a crack tip were reported by Altpeter et al. [32]; however, in their approach, BEMI was calibrated using XRD data.

3.2.2 Characterization of micro-residual stress by means of ultrasonic techniques

Residual stresses on the microscale require ultrasonic methods, which are characterized by a low interaction volume and high frequencies. A common method in research is scanning acoustic microscopy (SAM), which uses high-frequency ultrasonic waves >100 MHz to achieve lateral resolution in the range of 50–100 microns. By increasing the frequencies up to 1 GHz, the resolution is further improved. Surface waves or near-surface waves excited by such microscopes are used to determine the sound velocity and to map two-dimensional surface stress states [36]. To determine the absolute stress values, the sound velocity for the phase of the material to be examined must first be determined in calibration experiments, usually in tensile tests with parallel ultrasonic measurement. Since this can be a problem especially with polycrystalline materials due to local orientation differences, the method is also often used to represent only local anisotropy.

Based on the range of materials that can be examined, the use of a SAM is determined solely by the sound-damping properties [37]. Thus, therefore polymers and ceramic materials can be examined. Due to the small working distance and the sensitive sapphire or fused quartz lenses, a high surface quality and thus preparation are necessary.

Although the method has meanwhile lost in importance, current material developments in the field of functionalized and smart materials pose new challenges for the test methods that are used to describe their condition. Here, the SAM could be a useful extension, for example, to investigate non-metallic materials that are functionalized by the introduction of microscopic residual stress fields.

4. Conclusions

In this contribution, nondestructive methods are discussed with respect to their ability to characterize residual stresses. It is shown that there are approaches and testing situations where both ultrasonic and micromagnetic techniques are able to (at least quantitatively) determine residual stress. Nevertheless, the contribution clarifies that ultrasonic techniques are mainly used to determine macro-residual stress, whereas micromagnetic techniques are mainly used to determine micro-residual stresses. Most presented techniques, such as BEMI, 3MA, different EMAT applications, etc., are available for industrial use. New challenges can be found especially in the context of a depth-resolved determination of residual stresses.

Acknowledgements

The authors would like to thank the German Research Society for the financial support of research activities under grants Al 442/5-2, SCHM 746/71-2 and KI 1135/2-2.

Moreover, the authors would like to thank the Federal Ministry for Economic Affairs and Energy for the financial support of research activities under grant 1501523.

Notes/thanks/other declarations

The authors would like to thank Dr. Farajian for the performance of X-ray measurements on specimens made of 20MnMoNi5-5 steel.


Scientific innovation and technological progress can only be achieved when motivated people work together in a fruitful atmosphere. Only if these conditions are fulfilled and only if appropriate funding is provided, new technologies can be developed. Thus, the authors of this paper want to thank all funders and investors, all industrial and academic project partners as well as everyone who contributed in any way to the presented results.

Author details

Madalina Rabung*, Meisam Amiri, Michael Becker, Melanie Kopp, Ralf Tschuncky, Ines Veile, Fabian Weber, Miriam Weikert-Müller and Klaus Zielasko
Fraunhofer Institute for Nondestructive Testing IZFP, Saarbrücken, Germany

*Address all correspondence to: madalina.rabung@izfp.fraunhofer.de

IntechOpen

© 2020 The Author(s). Licensee IntechOpen. This chapter is distributed under the terms of the Creative Commons Attribution License (<http://creativecommons.org/licenses/by/3.0>), which permits unrestricted use, distribution, and reproduction in any medium, provided the original work is properly cited. 

References

- [1] Hosford W. Mechanical Behavior of Materials (2nd ed). New York: Cambridge University Press; 2010. p. 410
- [2] Macherauch E. Introduction to residual stress. In: Niku-Lari A, editor. *Advances in Surface Treatments Vol. IV - Residual stresses*. Oxford, New York, Frankfurt: Pergamon Press; 1987. pp. 1-36
- [3] Weiss P. L'hypothese du champ moléculaire et de la propriété ferromagnétique. *Journal de Physique*. 1907;6:661-690
- [4] Kneller E. *Ferromagnetismus*. Berlin, Heidelberg: Springer; 1962
- [5] Cullity BD. *Introduction to Magnetic Materials*. Boston: Addison-Wesley. ISBN: 0-201-01218-9; 1972
- [6] Tschuncky R. Sensor- und geräteunabhängige Kalibrierung elektromagnetischer zerstörungsfreier Prüfverfahren zur praxisorientierten Werkstoffcharakterisierung. PhD thesis (dissertation). Saarbrücken, Germany: Saarland University; 2011
- [7] Seeger A. *Moderne Probleme der Metallphysik*. Berlin, Heidelberg, New York: Springer; 1966
- [8] Barkhausen H. Zwei mit Hilfe der neuen Verstärker entdeckte Erscheinungen. *Physikalische Zeitschrift*. 1919;20:401-403
- [9] Altpeter I, Sklarzcyk C, Kopp M, Kröning M, Hübner S, Behrens BA. Nondestructive characterizing stress states in conventional deep drawing processes by means of electromagnetic methods. In: Shin Y-K et al., editors. *International Workshop on Electromagnetic Nondestructive Evaluation*. Amsterdam, Washington, Tokyo: IOS Press; 2009. pp. 131-139
- [10] Altpeter I, Becker R, Dobmann G, Kern R, Theiner WA, Yashan A. Robust solutions of inverse problems in electromagnetic non-destructive evaluation. *Inverse Problems*. 2002;18:1907-1921
- [11] Krautkrämer H, Krautkrämer J. *Werkstoffprüfung mit Ultraschall*. Berlin, Heidelberg, New York: Springer; 2013 (Nachdruck von 1986)
- [12] Niese F. EMUS-Wanddickensensor für die Pipeline-Inspektion mit integrierter Wirbelstrom- und Streuflussprüfung [Ph.D. thesis]. Saarbrücken: Universität des Saarlandes; 2010
- [13] Schneider E. Untersuchung der materialspezifischen Einflüsse und verfahrenstechnische Entwicklungen der Ultraschallverfahren zur Spannungsanalyse an Bauteilen [Ph.D. thesis]. Stuttgart: Fraunhofer IRB Verlag; 2000; ISBN 3-8167-5563-1
- [14] Schneider E, Herzer HR, Hübschen G, Wildau M, Steinhoff K. Bestimmung des oberflächennahen Spannungszustandes von Walzen in DGZfP-Jahrestagung 2009. *ZfP in Forschung, Entwicklung und Anwendung (2009)*. Deutsche Gesellschaft für zerstörungsfreie Prüfung (DGZfP); 2009
- [15] Withers PJ, Bhadeshia HKDH. Residual stress: part 1 – measurement techniques. *Materials Science and Technology*. 2001;17:355-365. DOI: 10.1179/026708301101509980
- [16] Hauk V. *Structural and Residual Stress Analysis by Nondestructive Methods*. Amsterdam: Elsevier; 1997. DOI: 10.1016/b978-0-444-82476-9.x5000-2.
- [17] Withers PJ, Bhadeshia HKDH. Residual stress: Part 2 – Nature and

- origins. *Materials Science and Technology*. 2001;17:366-375. DOI: 10.1179/026708301101510087
- [18] Kloos KH. Eigenspannungen, efinition und Entstehungsursachen. *Zeitschrift Werkstofftechnik*. 1997;10: 293-302. DOI: 10.1002/mawe.19790100906
- [19] Totten G, Howes M, Inoue T, editors. *Handbook of Residual Stress and Deformation of Steel*. Ohio: ASM International; 2002
- [20] Amiri M. *On the Microstructural Stress and Strain Behavior Determination of Metallic Materials Based on Electromagnetic Phenomena [Ph.D. Thesis]*. Saarbrücken: Saarland University; 2015
- [21] Hütte H. *Rückfederungsverhalten hochfester Stahlblechwerkstoffe beim Tiefziehen [PhD thesis]*. Universität Hannover; 2001
- [22] Doege E, Hütte H, Elend LE. 2nd Int. Conf. and Exhibition on Design and Prod. Of Dies and Molds. Turkey; 2001
- [23] Salzburger H J, Höller P. *Ultraschallprüfung an Komponenten bei Temperaturen bis 300°C*. 14. MPA-Seminar. Titel Hauptwerk: 14. MPA-Seminar '88. Sicherheit und Verfügbarkeit in der Anlagentechnik mit dem Schwerpunkt Langzeitintegrität der druckführenden Bauteile von Kernkraftwerken; 1988
- [24] Viktorov IA. *Rayleigh and Lamb Waves, Physical Theory and Applications*. New York: Plenum Press; 1967
- [25] Mora P, Spies M. In: *Inverse Problems: Inversion of Residual Stress Profiles from Ultrasonic Rayleigh Wave Dispersion Data*, Bristol: IOP Publishing; 34,055001, 2018
- [26] Weikert M, Niese F, Szielasko K. *Neue Ansätze zur Charakterisierung hochfester Stähle mittels geführter Ultraschallwellen*. in DGZfP-Jahrestagung 2014. ZfP in Forschung, Entwicklung und Anwendung (2014): Deutsche Gesellschaft für zerstörungsfreie Prüfung (DGZfP). Mi.2.B.4; 2014
- [27] Schneider E et al. Reliability assurance of railroad wheels by ultrasonic stress analysis. In: *European Conference on Residual Stresses*. Oberursel: DGM-Informationsgesellschaft; 1993. pp. 441-450. ISBN: 3-88355-192-9
- [28] *Residual Stresses in Railroad Commuter Car Wheels; Research Result*. US Department of Transportation-Federal Railroad Administration. RR99-01; April 1999
- [29] Tschuncky R, Rabung M, Youssef S, Farajian M, Luke M. Separation of residual stress and microstructure influences in nondestructive micromagnetic materials characterization for evaluation of power plant safety. Final report of Grant No. 1501523 in the frame of German national program for reactor safety; 2017
- [30] Altpeter I, Dobmann G, Kröning M, Rabung M, Szielasko K. Micro-magnetic evaluation of micro residual stresses of the IInd and IIIrd order. *NDT&E International*. 2009;42:283-290. DOI: 10.1016/j.ndteint.2008.11.007
- [31] Rabung M, Altpeter I, Boller C, Dobmann G, Herrmann HG. Non-destructive evaluation of the micro residual stresses of IIIrd order by using micro magnetic methods. *NDT&E International*. 2014;63:7-10. DOI: 10.1016/j.ndteint.2013.12.011
- [32] Altpeter I, Bender J, Hoffmann J, Kopp M. Barkhausen noise and eddy current microscopy, a new scanning probe technique for microscale characterization of materials. *Praktische Metallographie*. 1998;35(3):126-135

[33] Szielasko K, Lugin S, Kopp M, Altpeter I. Barkhausen noise and eddy current microscopy - a new scanning probe technique for microscale characterization of materials. In: Proc. of SPIE. Vol. 5392. Bellingham, WA; 2004. pp. 105-113

[34] Amiri M, Szielasko K, Altpeter I, Boller C, Fischer D, Hahn J. Point probes: A new generation of magnetic sensors for the measurement of local magnetic fields. In: Proc. of the 6th EEIGM Intl Conf on Adv Materials Research, IOP Conf Sereies 31. 2012. p. 012021. DOI: 10.1088/1757-899X/31/1/012021

[35] Augenstein E. Mikromagnetische Werkstoffcharakterisierung mit Punktsonden [thesis]. Germany: Fachhochschule Osnabrück; 2010

[36] Meeks SW et al. Microscopic imaging of residual stress using a scanning phase-measuring acoustic microscope. Applied Physics Letters. 1989;55:1835. DOI: 10.1063/1.102326

[37] Lee YC, Kim JO, Achenbach JD. Measurement of stresses by line-focus acoustic microscopy. Ultrasonics. 1994; 32(5):359-365. DOI: 10.1016/0041-624X(94)90105-8